Competing phases and orbital-selective behaviors in the two-orbital Hubbard-Holstein model

Shaozhi Li,[1] Ehsan Khatami,[2] and Steven Johnston[1,3,*]

[1]*Department of Physics and Astronomy, The University of Tennessee, Knoxville, Tennessee 37996, USA*
[2]*Department of Physics and Astronomy, San José State University, San José, California 95192, USA*
[3]*Leibniz-Institute for Solid State and Materials Research, Institute for Solid State Theory, IFW-Dresden, D-01171 Dresden, Germany*

(Dated: March 24, 2017)

We study the interplay between the electron-electron (*e-e*) and the electron-phonon (*e-ph*) interactions in the two-orbital Hubbard-Holstein model at half filling using the dynamical mean field theory. We find that the *e-ph* interaction, even at weak couplings, strongly modifies the phase diagram of this model and introduces an orbital-selective Peierls insulating phase (OSPI) that is analogous to the widely studied orbital-selective Mott phase (OSMP). At small *e-e* and *e-ph* couplings, we find a competition between the OSMP and the OSPI, while at large couplings, a competition occurs between Mott and charge-density-wave (CDW) insulating phases. We further demonstrate that the Hund's coupling influences the OSPI transition by lowering the energy associated with the CDW. Our results explicitly show that one must be cautious when neglecting the *e-ph* interaction in multi-orbital systems, where multiple electronic interactions create states that are readily influenced by perturbing interactions.

PACS numbers: 71.27.+a, 71.30.+h, 71.38.-k, 71.45.lr

arXiv:1703.03985v3 [cond-mat.str-el] 23 Mar 2017

Introduction — In recent years many researchers have focused on studying electron-electron (*e-e*) interactions in multiorbital systems such as the iron-based superconductors (FeSCs). In doing so, they have discovered numerous new phenomena, including the Hund's metal [1–3] and the orbital-selective Mott phase (OSMP) [4–8], which arise from the competing action of the electronic interactions. These concepts have helped shape our understanding of the enigmatic properties of these materials. Despite this success, however, surprisingly little is currently known about how competition/cooperation with other factors such as impurities or the electron-phonon (*e-ph*) interaction influences these phenomena. This question is important for our microscopic understanding of these materials, as subtle multiorbital correlation effects can produce states that are readily affected by small perturbations.

In the case of the FeSCs, the *e-ph* interaction was ruled out as a possible pairing mediator by early *ab initio* calculations [9] indicating that the total coupling strength was small, with a dimensionless *e-ph* coupling $\lambda \leq 0.2$. Because of this, many researchers have assumed that this interaction plays a secondary role in these materials with regards to other aspects as well. However, there is growing evidence that this outlook may have been premature. For example, more recent calculations find that taking into account the possible magnetism [10–13] or orbital fluctuations [14, 15] can increase the total *e-ph* coupling strength compared to the original estimates. This finding is consistent with the general notion that electron correlations can enhance *e-ph* interactions [16]. Moreover, the discovery of the FeSe films on oxide substrates [17] has implicated new possible lattice interactions, either across the interface [18, 19] or within the FeSe film [20]. Since bulk FeSe is believed to be in the OSMP regime [21, 22], these experiments naturally raise questions about when and how *e-ph* interactions can influence such multi-orbital phenomena.

Hubbard-Holstein models are the simplest models capturing the interplay between *e-e* and *e-ph* interactions. The single-band variant has been extensively studied, particularly at half-filling, where a direct competition occurs between antiferromagnetic Mott insulating (MI) and charge-density-wave (CDW) phases [23–32]. In comparison, far fewer studies exist for multiband generalizations of the model [14, 33]. Motivated by this, we carried out a dynamical mean field theory (DMFT) [34] study of a degenerate two-orbital Hubbard-Holstein model with inequivalent bandwidths. Here, we focus on the half-filled case and construct low-temperature phase diagrams in the λ-U and λ-J planes, where U and J are the Hubbard and Hund's interaction strengths, respectively. Similarly to the single-band case, we observe a competition between CDW and MI phases when the *e-ph* and *e-e* interactions are large. When the interactions are weak to intermediate in strength, however, we find additional phases displaying orbital-selective behavior. The first is the now well-studied OSMP driven by the electronic interactions [35]. The second is a lattice-driven analog of the OSMP, which we refer to as an orbital-selective Peierls insulator (OSPI). The phase boundaries of the model are also significantly influenced by the *e-ph* interaction, even for relatively weak values of $\lambda < 0.3$. This result clearly demonstrates that one cannot rule out the influence of the *e-ph* in correlated multiorbital systems *a priori* based on DFT-based estimates for the total cou-

pling strength.

Methods — The Hamiltonian for the degenerate two-orbital Hubbard-Holstein model [33] is $H = H_{\rm kin} + H_{\rm lat} + H_{\rm e-ph} + H_{\rm e-e}$, where

$$\begin{aligned} H_{\rm kin} &= -\sum_{\langle i,j\rangle,\gamma,\sigma} t_\gamma c^\dagger_{i,\gamma,\sigma} c_{j,\gamma,\sigma} - \mu \sum_{i,\gamma,\sigma} \hat{n}_{i,\gamma,\sigma}, \\ H_{\rm e-ph} + H_{\rm lat} &= g \sum_{i,\gamma,\sigma} \left(b^\dagger_i + b_i\right)\left(\hat{n}_{i,\gamma,\sigma} - \frac{1}{2}\right) + \Omega \sum_i b^\dagger_i b_i, \\ H_{\rm e-e} &= U \sum_{i,\gamma} \hat{n}_{i,\gamma,\uparrow}\hat{n}_{i,\gamma,\downarrow} + U' \sum_{i,\gamma\neq\gamma'} \hat{n}_{i,\gamma\uparrow}\hat{n}_{i,\gamma',\downarrow} \\ &\quad + (U' - J) \sum_{i,\gamma<\gamma',\sigma} \hat{n}_{i,\gamma,\sigma}\hat{n}_{i,\gamma',\sigma} \\ &\quad + J \sum_{i,\gamma\neq\gamma'} (c^\dagger_{i,\gamma,\uparrow} c^\dagger_{i,\gamma,\downarrow} c_{i,\gamma',\downarrow} c_{i,\gamma',\uparrow} \\ &\quad - c^\dagger_{i,\gamma,\uparrow} c_{i,\gamma,\downarrow} c^\dagger_{i,\gamma',\downarrow} c_{i,\gamma',\uparrow}) \end{aligned}$$

Here, $\langle\cdots\rangle$ denotes a summation over nearest neighbors; $c^\dagger_{i,\gamma,\sigma}$ creates an electron with spin σ in orbital $\gamma = 1, 2$ on site i; $b^\dagger_i$ creates a phonon on site i; $\hat{n}_{i,\gamma,\sigma} = c^\dagger_{i,\gamma,\sigma} c_{i,\gamma,\sigma}$ is the particle number operator; t_γ is the nearest neighbor hopping integral for orbital γ; U and U' are the intra- and inter-orbital Hubbard interactions, respectively. Throughout, we choose $U' = U - 2J$ due to rotational symmetry [2, 36]. J is the Hund's coupling, which is fixed to $J = U/5$ unless otherwise stated; g is the *e-ph* interaction strength; Ω is the phonon energy; and μ is the chemical potential, which is adjusted to fix the average particle per site to $\langle\hat{n}\rangle = 2$.

We studied the model using single-site DMFT [34], with exact diagonalization (ED) [37] as the impurity solver. DMFT maps the full lattice model with local interactions onto an impurity model embedded in a self-consistently determined host. In this case, the host is approximated using a set of $N_{\rm b} = 4$ discrete energy levels (results for $N_{\rm b} = 6$ are shown in the supplementary materials [38], where we find good convergence). We work in infinite dimensions (where DMFT is exact) by adopting a Bethe lattice with a semi-circular density of states $\rho_\gamma(\epsilon) = \frac{8}{\pi}\sqrt{(W_\gamma/2)^2 - \epsilon^2}/W_\gamma^2$, where $W_\gamma = 4t_\gamma$ is the bandwidth. Throughout the paper, we set $W_1 = 5W_2 \equiv W = 2$ eV, fix the temperature at $T = \frac{1}{\beta} = 0.01$ eV, unless otherwise stated, and set the phonon energy to $\Omega = 0.15$ eV. (Results for smaller values of Ω are qualitatively similar and can be found in Ref. [38].) The bandwidth and Hund's coupling J are chosen so that we can obtain a robust OSMP without the *e-ph* coupling. The dimensionless *e-ph* coupling constant is defined as $\lambda = \frac{2g^2}{W\Omega}$. The infinite phonon Hilbert space for the impurity model is limited by only allowing up to $N_{\rm ph}$ phonons, where $N_{\rm ph} \sim 40$ is typical, depending on the parameters used. We have checked that all of our results are well converged for increasing values of $N_{\rm ph}$.

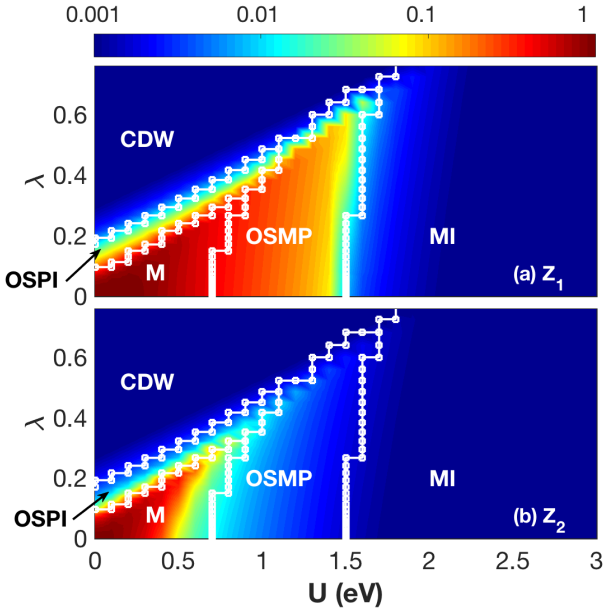

FIG. 1: (color online) The phase diagram for the two-orbital Hubbard-Holstein model in the *e-ph* interaction strength (λ) - Hubbard U plane at charge density $n = 2$ and temperature $\beta = 200/W$. (a) and (b) show density plots of quasiparticle weights Z_1 and Z_2 on a logarithmic scale, respectively. The different phases are labeled as follows: metal (M), orbital-selective Mott phase (OSMP), Mott insulater (MI), charge density wave (CDW), and orbital-selective Peierls insulator (OSPI). The white dots indicate points where the calculations were performed, and we plotted them to show phases boundaries. The color scale is plotted using a linear interpolation.

Results — The λ-U phase diagram for the model is shown in Fig. 1. Here, we plot the orbitally resolved Matsubara quasiparticle weight $Z_\gamma = \left(1 - \frac{{\rm Im}\Sigma({\rm i}\pi T)}{\pi T}\right)^{-1}$ on a logarithmic scale. Five distinct phases can be identified from the values of Z_γ, the local magnetic moment $m^2_{\gamma z} = \langle(n_{\gamma\uparrow} - n_{\gamma\downarrow})^2\rangle$, and the average number of phonon quanta $N_{\rm ph} = \langle b^\dagger b\rangle$ (all shown in Fig. 2), and their boundaries are indicated by the white lines. Three of these phases are similar to those found in the single-band Hubbard-Holstein model. The first phase is a metallic phase (M) at small (λ, U), where both Z_1 and Z_2 are large. The second is a Mott insulating (MI) phase, which appears at large U. It is identified by a situation where $Z_\gamma = 0$, the magnetic moments are large $m^2_{1,z} \approx m^2_{2,z} \approx 1$, and $N_{\rm ph}$ is nearly zero. The third phase is a CDW insulating phase where $Z_1 = Z_2 = 0$, while $N_{\rm ph}$ is large ($N_{\rm ph} \gg 1$) and no local moments have formed (i.e. $m^2_{1,z} \approx m^2_{2,z} \approx 0$). An examination of the wavefunctions reveals that the CDW phase corresponds to a state where the impurity site is either fully occupied or entirely empty with equal probability, consistent with a checkerboard-type ordering common to the single-

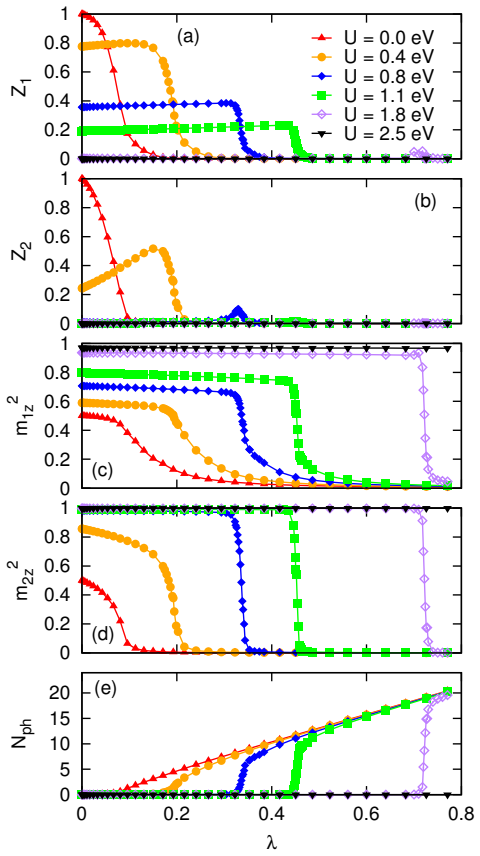

FIG. 2: (color online) The quasiparticle weights (a) Z_1 and (b) Z_2 as a function of the *e-ph* interaction strength (λ) at different Hubbard U values. Mean values of the local magnetic moments m^2_{1z}, m^2_{2z} and phonon numbers ($N_{\rm ph}$) are shown in (c), (d), and (e), respectively.

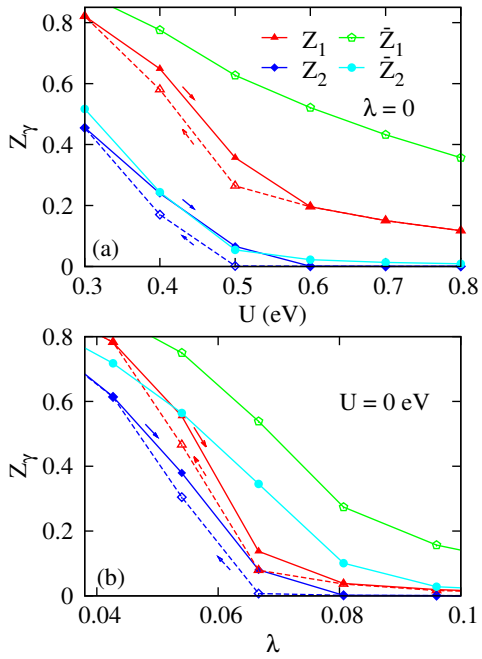

FIG. 3: (color online) (a) The quasiparticle weight Z_γ as a function of U at a fixed $\lambda = 0$. (b) The quasiparticle weight Z_γ as a function of λ at a fixed $U = 0$. Z_γ are results at $T = 0.002$ eV and $\bar{Z}_\gamma$ are results at $T = 0.01$ eV. The solid lines and the dashed lines are results of increasing and decreasing U or λ, respectively.

band model [23, 24, 26]. This phase is likely to be a $(\pi, \pi, ...)$ CDW order (sometimes referred to as a strong coupling bi-polaronic insulating phase in the single-band case). Alternatively, this phase could also reflect phase separation, although delocalization effects should favor the CDW. Further studies on extended clusters will be needed to address this issue.

In addition to the "standard" phases, we also observe two distinct phases with orbital selective characteristics. The first is the widely studied OSMP, which appears between the M and MI phases. It resembles the same OSMP found in the model without *e-ph* interactions [35]. Here, the orbital with the narrower bandwidth becomes insulating with $Z_2 = 0$ and $m^2_{2z} \approx 1$, while the orbital with the wider bandwidth remains itinerant with a non-zero quasiparticle weight. Interestingly, we also observe a second region of orbital selective behavior, located in a small portion of parameter space between the M/OSMP phases and the fully insulating CDW phase, denoted as OSPI in Fig. 1. As with the OSMP, in this region, the narrow band becomes insulating while the wide band remains itinerant with $Z_1 \neq 0$ and $Z_2 = 0$. But unlike the OSMP, here we find tiny local moments on orbital 2 with $m^2_{2z} \leq 0.05$, and a large $N_{\rm ph}$ ($N_{\rm ph} > 1$). The latter indicates the presence of a sizable lattice distortion. The *e-ph* interaction drives the orbital-selective insulating properties in this case rather than the Hubbard and Hund's interaction. We label this state an orbital selective Peierls insulator (OSPI), in analogy to the OSMP.

For reference, Fig. 2 shows the evolution of the quantities used to identify the five regions of the phase diagram as a function of λ for different values of U. When $U \leq 0.4$ eV, $m^2_{\gamma z}$ and $N_{\rm ph}$ vary smoothly near the phase transition, while for $U > 0.4$ eV, these quantities vary quickly in the transition region, but are nevertheless continuous. This behavior is consistent with a previous DMFT study of the single band Hubbard-Holstein model [24], where a smooth transition occurs at weak coupling that becomes increasingly sharp as U/W increases.

To study the analogy between the OSMP and the OSPI further, we examine the classification of the phase transitions and their possible hysteresis behavior [39]. Fig. 3(a) and 3(b) plot the evolution of Z_γ at $T = 0.002$ eV along the $(U, \lambda = 0)$ and $(U = 0, \lambda)$ axes, respectively. Although there are two Mott transitions in the two-orbital system, we observe a single hysteresis loop near the OSMP boundary, which indicates a coexistence region, as discussed in Ref. [39]. The critical U values for increasing and decreasing interaction strengths are

$U_{c,1} = 0.6$ eV and $U_{c,2} = 0.5$ eV, respectively. Similarly, along the $(U = 0, \lambda)$ line we also find a single coexistence region, consistent with DMFT studies for the single band Holstein model [40, 41]. As with the Mott transition, the hysteresis loop appears close to the first Peierls transition and the critical λ values for increasing and decreasing interactions are $\lambda_{c,1} = 0.08$ and $\lambda_{c,2} = 0.066$, respectively. Thus, the OSMP and OSPI transitions phenomena appear to be analogous to one another. The appearance of hysteresis indicates a first order transition out of the metallic phase while the other transitions are continuous. Finally, we note that the hysteresis behavior disappears at $T = 0.01$ eV, where we performed most of our calculations.

The Hund's coupling plays a major role in establishing the boundaries of the OSMP [5, 42]. Therefore, we explored its role in determining the CDW and OSPI phases observed here. Fig. 4 shows the phase diagram in the λ - J/U plane for a fixed $U = 0.8$ eV. For $\lambda < 0.3$, the metallic phase survives to larger values of J/U as λ increases. This result is consistent with the notion that the *e-ph* interaction mediates an effective attractive interaction that competes with the onsite Hubbard interactions. When $0.3 < \lambda < 0.4$, the OSMP disappears and is replaced by the OSPI and CDW phases and the critical λ value for both phases is decreased as J/U increases. For larger λ, the CDW phase persists for all J/U values. Thus, the Hund's coupling not only favors the OSMP transition but also has a stabilizing effect for the lattice-driven phases.

In the single band Hubbard-Holstein model, the action of the repulsive Hubbard interaction and the effective attractive interaction mediated by the phonons gives rise to the competition between CDW and MI phases. Here, in the multi-orbital case, the stabilization of the CDW phase with increasing J/U is due to the reduction of the interorbital Hubbard interaction, imposed by the condition that $U' = U - 2J$. In short, increasing J reduces U' and therefore also reduces the total potential energy cost for a double occupation of a given site. The cost for creating a charge ordered phase, where each site alternates between fully occupied and empty, is therefore lowered. This interpretation can be confirmed explicitly by holding U and U' fixed while varying J. The corresponding phase diagram does not show the same stabilization of the CDW phase with increasing J [38].

We have studied the interplay between the *e-e* and *e-ph* interactions in a degenerate two-orbital Hubbard-Holstein model. A Competition between the onsite *e-e* and *e-ph* interactions leads to many competing phases including the OSMP and OSPI at small couplings and the MI and CDW at large couplings. We also find that the Hund's coupling J has nontrivial effects on the phases driven by the *e-ph* interactions. Importantly, our results demonstrate that weak to intermediate *e-ph* interaction strengths can have a significant impact on the phase diagram of this model. As such, one cannot rule out an important role for phonons *a priori* in multi-orbital systems, where multiple electronic interactions are already competing with one another.

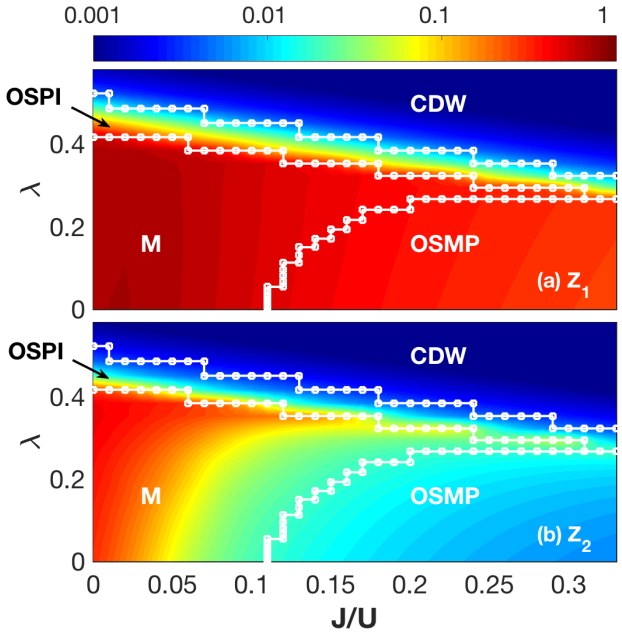

FIG. 4: (color online) The phase diagram in the λ-J/U plane at filling $n = 2$. (a) and (b) plot quasiparticle weights Z_1 and Z_2, respectively. The labels used in this graph are the same as in Fig. 1. The Coulomb interaction is fixed at $U = 0.8$ eV and $U' = U - 2J$. The white dots indicate points where the calculations were performed, and we plotted them to show phases boundaries. The color scale is plotted using a linear interpolation.

We close with a short note and some speculation. Ref. [43] has also used the term OSPI in the context of a two-orbital dimer model, where superexchange is stronger between a particular subset of orbitals, creating a preferential dimerization. An entirely different mechanism drives our OSPI, where we start from a metallic state and obtain the OSPI through the *e-ph* interaction. To the best of our the knowledge, this is the first time that theoretical calculations have produced such a mechanism. As with OSMP, the OSPI, in this case, is induced by the different bandwidths for the two orbitals. Finally, although the OSPI discovered here was derived from a Holstein coupling, we believe bond-stretching phonons that modulate interatomic hopping integrals could induce a similar phenomenon. In such cases, these interactions could have a significant impact on nematic phases observed in some FeSCs [44, 45].

Acknowledgments — This work was supported by the University of Tennessee's Science Alliance Joint Directed Research Development (JDRD) program, a collaboration with Oak Ridge National Laboratory. S. J. also acknowledges support from the German Research Foundation (DFG) under SFB 1143 and hos-

pitality of the IFW-Dresden. E. K. is supported by the National Science Foundation Grant No. DMR-1609560. CPU time was provided by resources supported by the University of Tennessee and Oak Ridge National Laboratory Joint Institute for Computational Sciences (http://www.jics.utk.edu).

* Electronic address: sjohn145@utk.edu

[1] K. Haule and G. Kotliar, New J. Phys. **11**, 025021 (2009).
[2] A. Georges, L. de' Medici, and J. Mravlje, Annu. Rev. Condens. Matter Phys. **4**, 137 (2013).
[3] L. Fanfarillo and E. Bascones, Phys. Rev. B **92**, 075136 (2015).
[4] V. I. Anisimov, I. A. Nekrasov, D. E. Kondakov, T. M. Rice, and M. Sigrist, Eur. Phys. J. B **25**, 191 (2002).
[5] A. Koga, N. Kawakami, T. M. Rice, and M. Sigrist, Phys. Rev. Lett. **92**, 216402 (2004).
[6] L. de'Medici, G. Giovannetti, and M. Capone, Phys. Rev. Lett. **112**, 177001 (2014).
[7] M. Yi, D. H. Lu, R. Yu, S. C. Riggs, J.-H. Chu, B. Lv, Z. K. Liu, M. Lu, Y.-T. Cui, M. Hashimoto, S. -K. Mo, Z. Hussain, C. W. Chu, I. R. Fisher, Q. Si, and Z.-X. Shen, Phys. Rev. Lett. **110**, 067003 (2013).
[8] S. Li, N. Kaushal, Y. Wang, Y. Tang, G. Alvarez, A. Nocera, T. A. Maier, E. Dagotto, and S. Johnston, Phys. Rev. B **94**, 235126 (2016).
[9] L. Boeri, O. V. Dolgov, and A. A. Golubov, Phys. Rev. Lett. **101**, 026403 (2008).
[10] F. Yndurain and J. M. Soler, Phys. Rev. B **79**, 134506 (2009)
[11] L. Boeri, M. Calandra, I. I. Mazin, O. V. Dolgov, and F. Mauri, Phys. Rev. B **82**, 020506 (2010).
[12] S. Coh, M. L. Cohen, and S. G. Louie, Phys. Rev. B **94**, 104505 (2016).
[13] S. Mandal, R. E. Cohen, and K. Haule, Phys. Rev. B **89**, 220502 (2014).
[14] H. Kontani and S. Onari, Phys. Rev. Lett. **104**, 157001 (2010).
[15] T. Saito, S. Onari, and H. Kontani, Phys. Rev. B **82**, 144510 (2010).
[16] M. Capone, C. Castellani, and M. Grilli, Adv. Condens. Matter Phys. **2010**, 920860 (2010).
[17] Q. L. Wang *et al.*, Chin. Phys. Lett. **29**, 037402 (2012).
[18] J. J. Lee *et al.*, Nature (London) **515**, 245 (2014).
[19] L. Rademaker, Y. Wang, T. Berlijn, and S. Johnston, New. J. Phys. **18**, 022001 (2016).
[20] S. Coh, M. L. Cohen, and S. Louie, New J. Phys. **17**, 073027 (2015).
[21] M. D. Watson, S. Backes, A. A. Haghighirad, M. Hoesch, T. K. Kim, A. I. Coldea, and R. Valenti, Phys. Rev. B **95**, 081106 (2017).
[22] D. V. Evtushinsky, M. Aichhorn, Y. Sassa, Z.-H. Liu, J. Maletz, T.Wolf, A. N.Yaresko, S. Biermann, S. V. Borisenko, and B. Büchner, arXiv:1612.02313.
[23] J. Bauer, EPL **90**, 27002 (2010).
[24] J. Bauer and A. C. Hewson, Phys. Rev. B **81**, 235113 (2010).
[25] E. Berger, P. Valášĕk, and W. von der Linden, Phys. Rev. B **52**, 4806 (1995).
[26] E. A. Nowadnick, S. Johnston, B. Moritz, R. T. Scalettar, and T. P. Devereaux, Phys. Rev. Lett. **109**, 246404 (2012).
[27] Y. Murakami, P. Werner, N. Tsuji, and H. Aoki, Phys. Rev. B **88**, 125126 (2013).
[28] P. Werner and M. Eckstein, Phys. Rev. B **88**, 165108 (2013).
[29] G. Sangiovanni, O. Gunnarsson, E. Koch, C. Castellani, and M. Capone, Phys. Rev. Lett. **97**, 046404 (2006).
[30] A. Macridin, B. Moritz, M. Jarrell, and T. Maier, Phys. Rev. Lett. **97**, 056402 (2006).
[31] A. Nocera, M. Soltanieh-ha, C. A. Perroni, V. Cataudella, and A. E. Feiguin, Phys. Rev. B **90**, 195134 (2014).
[32] E. Khatami, A. Macridin, and M. Jarrell, Phys. Rev. B **78**, 060502 (2008).
[33] T. Yamada, J. Ishizuka, and Y. Ōno, J. Phys. Soc. Jpn. **83**, 044711 (2014).
[34] A. Georges, G. Kotliar, W. Krauth, and M. J. Rozenberg, Rev. Mod. Phys. **68**, 13 (1996).
[35] Luca de' Medici, Phys. Rev. B **83**, 205112 (2011).
[36] C. Castellani, C. Di Castro, D. Feinberg, and J. Ranninger, Phys. Rev. Lett. **43**, 1957 (1979).
[37] A. Liebsch and H. Ishida, J. Phys.: Condens. Matter **24**, 053201 (2012).
[38] For a complete description of our implementation of DMFT and additional results concerning the model, see the supplementary materials.
[39] A. Liebsch, Phys. Rev. B **70**, 165103 (2004).
[40] D. Meyer, A. C. Hewson, and R. Bulla, Phys. Rev. Lett. **89**, 196401 (2002).
[41] G. S. Jeon, T. -H. Park, J. H. Han, H. C. Lee, and H. -Y. Choi, Phys. Rev. B **70**, 125114 (2004).
[42] Luca de' Medici, S. R. Hassan, M. Capone, and X. Dai, Phys. Rev. Lett. **102**, 126401 (2009).
[43] S. V. Streltsov and D. I. Khomskii, Phys. Rev. B **89**, 161112 (2014).
[44] J.-H. Chu, H.-H. Kuo, J. G. Analytis, and I. R. Fisher, Science, **337**, 710 (2012).
[45] J. P. Sun, K. Matsuura, G. Z. Ye, Y. Mizukami, M. Shimozawa, K. Matsubayashi, M. Yamashita, T. Watashige, S. Kasahara, Y. Matsuda, J. -Q. Yan, B. C. Sales, Y. Uwatoko, J. -G. Cheng, and T. Shibauchi, Nature Comm. **7**, 12146 (2016).